Probing hot-electron effects in wide area plasmonic surfaces using X-ray photoelectron spectroscopy

Sencer Ayas, Andi Cupallari, and Aykutlu Dana

Citation: Appl. Phys. Lett. **105**, 221608 (2014);
View online: https://doi.org/10.1063/1.4903295
View Table of Contents: http://aip.scitation.org/toc/apl/105/22
Published by the American Institute of Physics

Articles you may be interested in

Aluminum-based hot carrier plasmonics
Applied Physics Letters **110**, 021117 (2017); 10.1063/1.4973814

Coaxial Ag/ZnO/Ag nanowire for highly sensitive hot-electron photodetection
Applied Physics Letters **106**, 081109 (2015); 10.1063/1.4913613

Solar energy conversion via hot electron internal photoemission in metallic nanostructures: Efficiency estimates
Journal of Applied Physics **115**, 134301 (2014); 10.1063/1.4870040

Surface-plasmon enhanced photodetection at communication band based on hot electrons
Journal of Applied Physics **118**, 063101 (2015); 10.1063/1.4928133

Probing polarization modes of Ag nanowires with hot electron detection on Au/TiO_2 nanodiodes
Applied Physics Letters **102**, 123112 (2013); 10.1063/1.4799156

Long-range Tamm surface plasmons supported by graphene-dielectric metamaterials
Journal of Applied Physics **121**, 033101 (2017); 10.1063/1.4973900

Probing hot-electron effects in wide area plasmonic surfaces using X-ray photoelectron spectroscopy

Sencer Ayas,[a] Andi Cupallari,[a] and Aykutlu Dana[b]
UNAM Institute of Materials Science and Nanotechnology, Bilkent University, 06800 Ankara, Turkey

(Received 7 August 2014; accepted 21 November 2014; published online 5 December 2014)

Plasmon enhanced hot carrier formation in metallic nanostructures increasingly attracts attention due to potential applications in photodetection, photocatalysis, and solar energy conversion. Here, hot-electron effects in nanoscale metal-insulator-metal (MIM) structures are investigated using a non-contact X-ray photoelectron spectroscopy based technique using continuous wave X-ray and laser excitations. The effects are observed through shifts of the binding energy of the top metal layer upon excitation with lasers of 445, 532, and 650 nm wavelength. The shifts are polarization dependent for plasmonic MIM grating structures fabricated by electron beam lithography. Wide area plasmonic MIM surfaces fabricated using a lithography free route by the dewetting of evaporated Ag on HfO_2 exhibit polarization independent optical absorption and surface photovoltage. Using a simple model and making several assumptions about the magnitude of the photoemission current, the responsivity and external quantum efficiency of wide area plasmonic MIM surfaces are estimated as 500 nA/W and 11×10^{-6} for 445 nm illumination. © *2014 AIP Publishing LLC*. [http://dx.doi.org/10.1063/1.4903295]

Plasmonic structures have attracted increasing attention in the recent years, enabling engineering of optical properties of surfaces.[1–3] Hot-electron effects (HEE) in plasmonic structures have been investigated as alternative mechanisms for solar energy harvesting and photodetection.[4–8] HEE rely on transfer of hot carriers from one contact to another through a thin dielectric barrier and provide a semiconductor free route for the photoconversion. A relevant thin film structure is the metal-insulator-metal (MIM) configuration, where optical properties of the surface can be tuned through plasmonic resonances, while separately allowing engineering of carrier transfer and collection. Hot-electron transfer competes with thermalization in the conversion of the absorbed light into a DC or voltage.[9,10] The transient electron energy distributions of metallic surfaces excited by light pulses are thermalized in short time scales ranging from 100 fs to 1 ps. Photoelectron emission with pulsed X-ray, UV, and visible light sources was used in investigation of non-equilibrium energy distributions of carriers on surfaces.[11–13] Such pulsed or pump-probe measurements provide direct information about carrier dynamics, however require advanced light sources. X-Ray Photoelectron Spectroscopy (XPS) was used to investigate surface photovoltaic and photoconductivity effects in nanocomposite surfaces without using femtosecond or picoseconds light or X-ray pulses.[14–18] Here, we extend such use of XPS to investigate HEE in plasmonic MIM structures. Laser excitation is used to illuminate the plasmonic surfaces (Figure 1(a)). The top metal of the MIM structures acts as the plasmonic antenna (metal nanodiscs or gratings/stripes) that provides enhanced optical absorption. Plasmonic enhancement leads to more efficient hot-electron generation. HEE result in surface photovoltages and are observed by comparing shifts of binding energy (BE) of the top metal islands for dark and illuminated conditions.

A schematic description of the band diagram of a MIM surface under X-ray and visible light illumination is shown in Figure 1(b). A top metal layer, Ag, is separated from a bottom metal layer by a thin dielectric barrier. Under X-ray illumination, the photoelectrons that escape from the top metal islands result in a positive current (J_x), charging the surface positively (Figure 1(a)). As a consequence, band bending occurs as shown in Figure 1(b). In the absence of a compensating electron gun, the surface potential reaches steady-state due to the presence of direct (or trap assisted) tunneling current from the bottom metal to the surface, denoted by J_t in Figure 1(b). When the surface is illuminated, absorption takes place at the top and bottom metals and the hot-electrons acquire an energy distribution, as shown by rectangles in Figure 1(b) on both sides of the junction. The electron mean free path is on the order of 20–30 nm, which is longer than the dielectric thickness. Therefore, hot-electrons with energies greater than the barrier height can be partially transmitted towards the top metal island where they are thermalized.[9] This causes a negative shift of the observed BE of Ag. In contrast, hot-electrons generated in the top metal layer are not able to tunnel from the positively charged island.

Recently, a nanostripe antenna was used to demonstrate plasmonic hot-electron current enhancement in MIM devices.[23] Polarization dependence of the enhancement was measured to show that optical absorption in the metal layers was dominated by plasmonic effects. Here, we demonstrate that HEE related surface photovoltages can be measured in similar MIM structures using XPS. Periodic MIM structures are fabricated using standard techniques. A 70 nm thick Ag layer is covered with 5 nm HfO_2, deposited using Atomic Layer Deposition (ALD) at 100 °C. Metal stripes are patterned by electron beam lithography and lift-off, resulting in 50 nm thick Ag stripes. The width, period, and length of the stripes

[a]S. Ayas and A. Cupallari contributed equally to this work.
[b]E-mail: aykutlu@unam.bilkent.edu.tr

 © 2014 AIP Publishing LLC

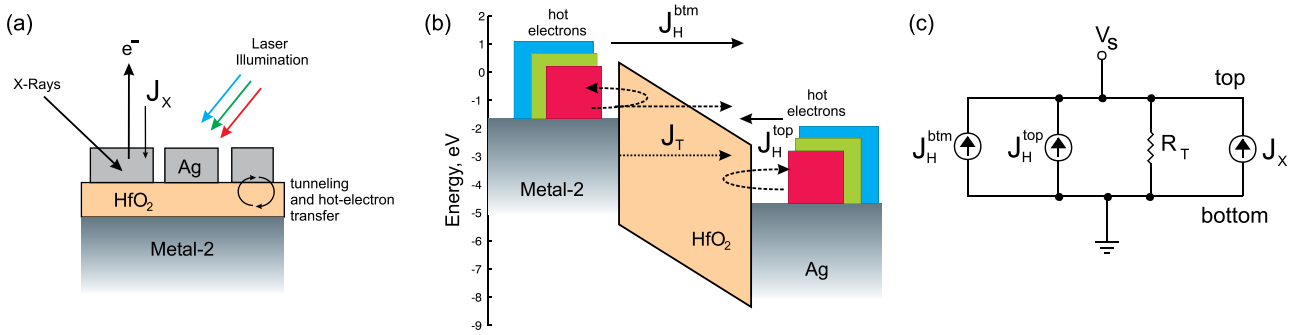

FIG. 1. (a) Cross-section of the MIM surface during an XPS measurement with laser illumination. J_x represents the X-ray induced photoemission current into the vacuum. (b) The band diagram of the MIM junction under X-ray and laser illumination. Hot-electron energy distributions are shown with rectangles above the Fermi level, due to absorption of light in the top and bottom metal layers. (c) A simplified circuit model with various currents acting on the top metal layer which acquires a steady state voltage of V_s. Current J_T through the dielectric is modeled within a first order approximation by the resistor R_T.

are 150 nm, 250 nm, and 50 μm, respectively. The area of the patterns (250 μm^2) matches the XPS data collection spot size. In order to elucidate the plasmonic nature of absorption in the metal layers, two grating structures perpendicular to each other are fabricated (Figure 2(a)). The MIM gratings feature wide angle and localized resonances in their optical response.[19] Field localization is calculated using Finite-Difference Time-Domain (FDTD) simulations for the TE and TM polarizations (Figure 2(b)). The plasmonic absorption P_a in the metal layers is resistive and location dependent, $P_a(r) = \langle \vec{j}(r) \cdot E(\vec{r}) \rangle = \frac{1}{2}\epsilon_0 \epsilon_i \omega |E(r)|^2$, where $\vec{j}(r)$ is the current density, ϵ_0 is the vacuum electric permittivity, ϵ_i is the imaginary part of the relative electric permittivity of the metal, ω is the angular frequency, and E(r) is the local electric field. Total absorption can be calculated by integrating the absorbed power over the material boundaries. It is seen in Figure 2(b) that TE polarization does not excite the plasmonic mode and little or no field penetrates the metal within the gap region. In this case, hot-electron generation is minimal. In contrast, TM polarization excites the plasmonic resonance and enhances hot-electron generation in the top and bottom metal layers, within the regions facing the dielectric gap. The hot-electrons tunnel across the dielectric and disturb the charge equilibrium of the surface Ag layers and cause shifts in the apparent BE of Ag under 532 nm illumination at 40 mW/mm^2 (Figure 2(c)). The workfunction of Ag is assumed to be 4.7 eV. The HfO_2/Ag conduction band barrier is 2.05 eV and this facilitates partial tunneling of hot-electrons for the used laser wavelengths 445 nm (2.77 eV), 532 nm (2.34 eV), and 650 nm (1.92 eV).[20] The laser is incident at 45° and the polarization can be chosen to be parallel or at an angle to the surface plane by a polarizer. Under dark conditions, the Ag 3d peaks whose native binding energies are 374.35 eV (Ag $3d_{3/2}$) and 368.24 eV (Ag $3d_{5/2}$) are shifted towards positive energies (to 370.2 eV for the Ag $3d_{5/2}$ peak) due to X-Ray induced charging. When the polarization has a vertical component, a negative BE shift is observed for the grating that is perpendicular to the light propagation vector (from 370.2 eV to 369.1 eV for the Ag $3d_{5/2}$ peak, II in Figure 2(c)), while the gratings parallel to the excitation (I in Figure 2(c)) do not exhibit a significant shift. When the polarization is rotated, the responses of the periodic stripe antennas are reversed, highlighting the plasmonic origin of the observed shifts.

In order to demonstrate that HEE can be observed in wide area plasmonic surfaces, we use spontaneously organized MIM surfaces (Figure 3(a)). The surfaces are fabricated by depositing 5 nm thick ALD deposited HfO_2 (at 100 °C) on

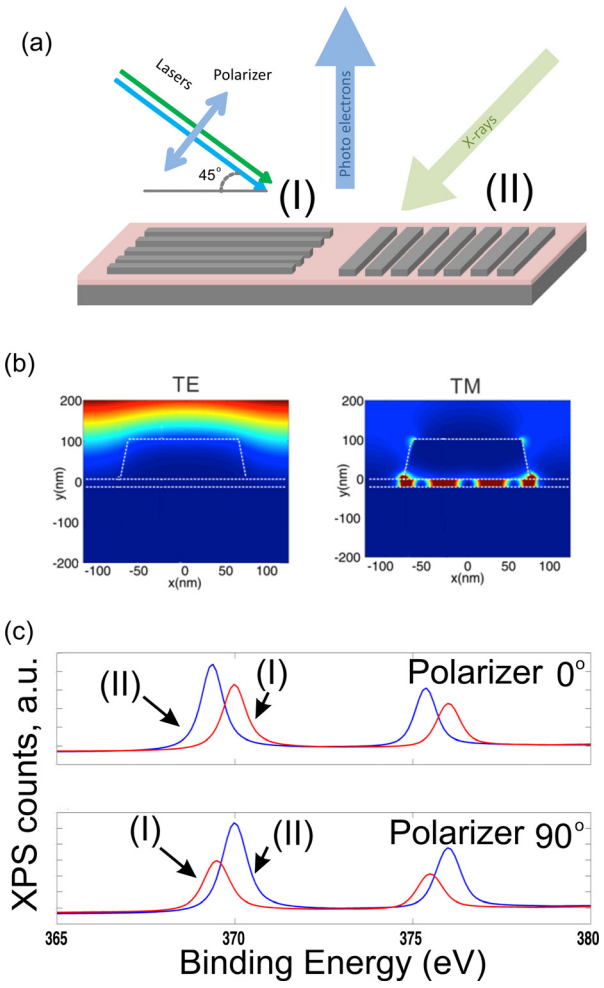

FIG. 2. (a) Schematic description of the MIM grating structures used in polarization dependent measurements. (b) Calculated field profiles of the structures for TE and TM polarizations. Field enhancement is minimal for TE polarization, while plasmonic enhancement is present in the gap for TM polarization. (Scale bar 50 nm). (c) XPS spectra of the Ag 3d peaks acquired on gratings labeled as (I) and (II) for two polarizer orientations. As the polarizer is rotated from 0° to 90°, apparent binding energy shifts of the Ag $3d_{3/2}$ and $3d_{5/2}$ are observed for the gratings with different orientations. Each polarization excites only one of the gratings, for which the plasmonic modes are excited.

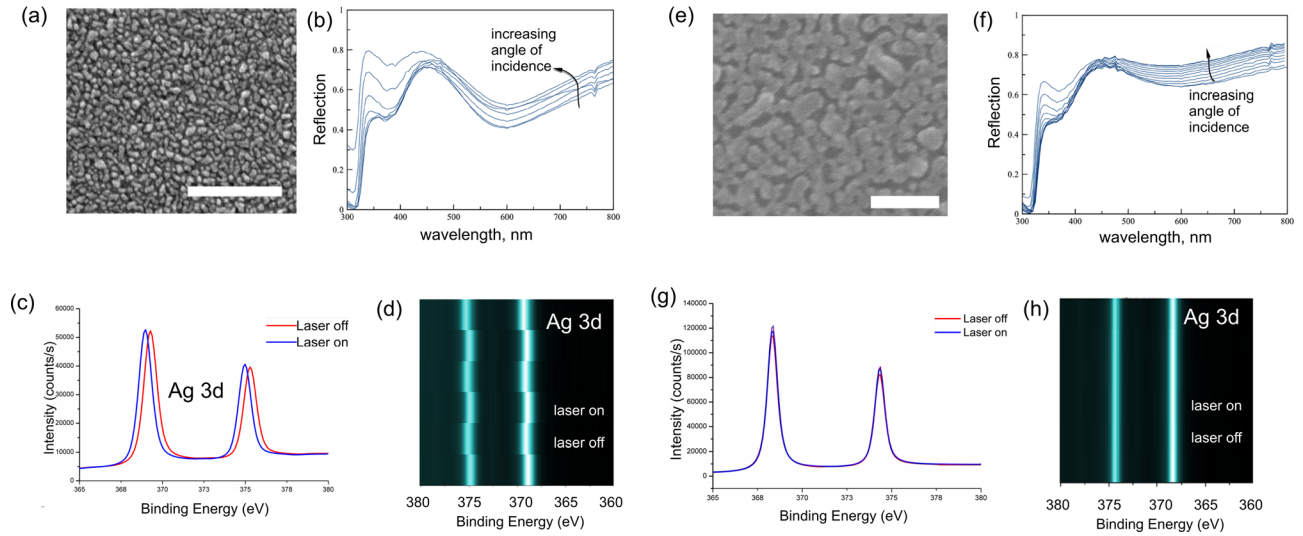

FIG. 3. (a) Scanning electron micrograph of MIM surface fabricated by atomic layer deposition of HfO_2 on Ag and self-organized formation of Ag nanoislands on HfO_2 upon 3 nm thick Ag evaporation (Scale bar 250 nm). (b) Reflectance of the surfaces for incidence angles ranging from 20° to 80° shows a broad plasmonic absorption peak around 580 nm. (c) Photo-response of the MIM surface when illuminated by 532 nm excitation, measured by XPS. (d) Consecutive measurements of the XPS spectrum under dark and illuminated conditions exhibit repeatable differential shifts of the Ag 3d lines. (e)–(h) Same as in (a)–(d) except the top Ag mass thickness is 5 nm and a semicontinuous Ag film is formed instead of MIM nanoislands and no surface photovoltage is observed.

an 80 nm thick Ag layer on silicon. A thin Ag layer of 3 nm mass thickness is evaporated on the HfO_2, which forms Ag nanoislands of average diameter of 30 nm and thickness of 10 nm.[21,22] The surface exhibits a broad plasmonic absorption band around 580 nm (Figure 3(b)) and a repeatable photoresponse as measured by XPS, as shown in Figures 3(c) and 3(d). When a semicontinuous film is formed on top of HfO_2 by depositing 5 nm thick Ag, no photoresponse can be observed (Figures 3(e)–3(h)). The lack of surface photovoltage in the 5 nm Ag case is attributed to reduced plasmonic absorption and lower density of openings in the film where the excitation can couple to into modes between the metal layers. When the surface is illuminated by lasers of wavelength 445, 532, and 650 nm (22 mW/mm^2), the BE shifts on the 3 nm Ag surface are observed to be dependent on photon energy (Figure 4(a)). The observed binding energies are shifted from 370.2 eV for the Ag $3d_{5/2}$ under dark conditions to 369.01 ± 0.03 eV for 445 nm, 369.33 ± 0.03 eV for 532 nm, and 369.81 ± 0.03 eV for 650 nm excitation. The apparent BE is dependent on excitation power (Figure 4(b)) for 445 nm excitation at 5, 10, and 20 mW/mm^2. The shifts, with respect to observed BE under dark conditions (at 370.2 eV), are towards the native (grounded, bulk) BE of Ag $3d_{5/2}$ at 368.4 eV and increase with increasing excitation power density, saturating at high intensities.

The observations can be understood in terms of steady state currents, including hot-electron, tunneling, and photoemission currents. The IV characteristics of MIM junctions under illumination have been previously studied in the context of energy harvesting and photodetection. If no other internal current sources are present, the open circuit voltage is independent of excitation power and is given by[7]

$$V_{OC} = -\frac{h\nu - \varphi_e}{e} \times \left[1 - J_H^{btm}/J_H^{top}\right], \tag{1}$$

where J_H's and V_{oc} are hot-electron currents and open-circuit voltage, $h\nu$ is the photon energy, φ_e is the barrier height, and e is the electronic charge. In the case of the MIM junction illuminated by light and X-rays, the photoelectron current J_x must also be included in calculation of the equilibrium condition. For $V_S > 0$, i.e., a net positive charging of the top islands, the hot-electron currents can be written as $J_H^{btm} = -\gamma P_a^{btm}(h\nu - \varphi_e)/h\nu$ and $J_H^{top} = \gamma P_a^{top}\max(h\nu - \varphi_e - eV_S, 0)/h\nu$, where P_a^{btm} and P_a^{top} are the absorbed power at the bottom and

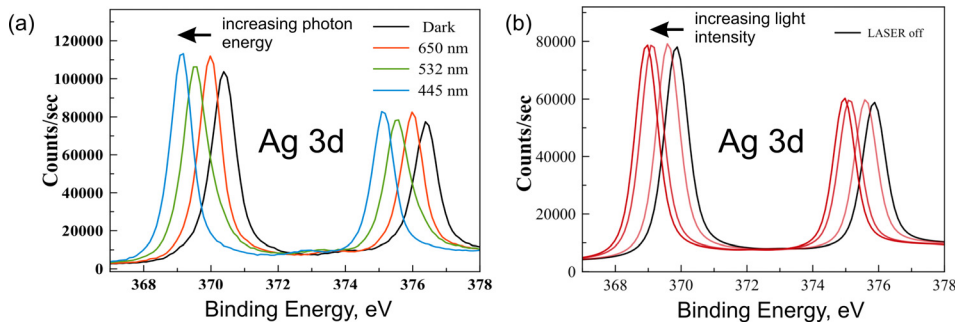

FIG. 4. (a) XPS spectra of the Ag 3d peaks measured on the MIM surface for dark and illuminated conditions, using lasers of 650, 532, and 445 nm wavelength, 20 mW power. The binding energies shift to negative due to hot-electron tunneling from the bottom metal to the top Ag island. Greater shifts are observed for increasing photon energy. (b) As the illumination intensity (445 nm) is increased from 5 to 20 mW, greater negative shift of the binding energy is observed which saturates at high intensities.

top metal. Here, γ is a proportionality constant, which is included to approximately take into account the hot-electron density and velocity inside the metals. Assuming the surface is positively charged, i.e., $V_S > 0$, the circuit diagram in Figure 1(c) can be used to infer the steady state surface voltage V_S. For V_S larger than $(E_{ph} - \varphi_e)/e \approx 0.72$ V for 445 nm illumination, all hot-electrons from the top metal are assumed to be reflected and $J_{sc}^{top} \approx 0$. It was demonstrated that the dielectric behaves as a resistive layer under X-ray exposure, due to continuous ionization within the layer.[24,25] Resistance of a 4 nm thick SiO_2 layer was determined to be 8.0 ± 1.0 MΩ in an XPS measurement specifically designed to extract electronic properties. We assume that the HfO_2 layer behaves similarly, like both a tunnel barrier for hot-electrons and a Poole-Frenkel conductor, i.e., $J_t \cong V_S/R_t$. A more accurate quantitative analysis requires direct measurement of the photoelectron current or effective resistance of the HfO_2 layer (as done in Ref. 24). The circuit model is still relevant for providing a qualitative understanding of the observed shifts. The steady state condition for $V_S > 0$ is

$$J_x + \gamma P_a^{top} \frac{\max(h\nu - \varphi_e - eV_S, 0)}{h\nu} - \gamma P_a^{btm} \frac{h\nu - \varphi_e}{h\nu} = \frac{V_S}{R_T}, \tag{2}$$

which predicts a surface voltage of $V_S = R_T J_x$ for dark conditions ($P_a^{top} = P_a^{btm} = 0$). For the case of high power illumination ($P_a^{top}, P_a^{btm} \to \infty$), Eq. (2) predicts a surface voltage $V_S = \frac{h\nu - \varphi_e}{e} \times \left[1 - P_a^{btm}/P_a^{top}\right]$, which is equivalent to the open circuit voltage given in Eq. (1). Using $J_x \approx 72$ nA/mm^2 measured for a similar XPS system, we estimate the resistance of the 5 nm thick HfO_2 layer as 25 MΩ over 1 mm^2 surface area. According to the data shown in Figure 4(b) for 445 nm excitation, 5 mW incident power causes a surface voltage shift of 256 mV over a 300 μm diameter illumination area, corresponding to a hot-electron current of 2.5 nA. The current is used to estimate the external quantum efficiency (EQE) as 11×10^{-6} and responsivity as 500 nA/W, for the 300 μm diameter measurement area. The calculated responsivity compares favorably with the 75 nA/W measured for the same wavelength in stripe nanoantenna devices.[23] At higher excitation densities at 445 nm (Figure 4(b)), the surface voltage approaches 0.54 V, which would require a J_H^{btm}/J_H^{top} ratio of 0.25 according to Eq. (1).

In conclusion, we demonstrated that quasi-static XPS measurements can be used to observe and investigate HEE on plasmonic surfaces. The assumptions about the circuit model element values lead to EQE and responsivity values that are in agreement within the same order of magnitude of previously reported MIM devices. One issue that must be noted is: hot-electron currents are expected to be minimal for red laser excitation (1.92 eV), due to sufficiently large HfO_2 conduction band barrier (2.02 eV). The observation of surface photovoltages for this wavelength is either due to reduced conduction band barrier for the HfO_2 material deposited in our facility or due to the involvement of hot-electrons that are excited from trap states inside the HfO_2 barrier. These observations suggest that the model we present here is basic and more advanced modeling must be used to better understand the dependence of the surface photovoltage on experimental parameters. In a recent article, surface photovoltages have been observed in arrays of gold nanoparticles on an indium tin oxide substrate using Kelvin Probe Force Microscopy (KPFM).[26] In contrast, the non-contact method we demonstrated here to study surface photovoltages in plasmonic nanostructures does not require a proximal probe and possesses the additional benefit of chemical resolution due to the use of XPS.

This work was partially supported by TUBITAK under Grant No. 111M344, EU FP7: People-IAPP NanoBacterPhageSERS.

[1]S. A. Maier and H. A. Atwater, J. Appl. Phys. **98**(1), 011101 (2005).
[2]J. A. Schuller, E. S. Barnard, W. Cai, Y. C. Jun, J. S. White, and M. L. Brongersma, Nat. Mater. **9**(3), 193–204 (2010).
[3]H. A. Atwater and A. Polman, Nat. Mater. **9**(3), 205–213 (2010).
[4]F. Wang and N. A. Melosh, Nat. Commun. **4**, 1711 (2013).
[5]K. Kempa, M. J. Naughton, Z. F. Ren, A. Herczynski, T. Kirkpatrick, J. Rybczynski, and Y. Gao, Appl. Phys. Lett. **95**(23), 233121 (2009).
[6]M. A. Green, Prog. Photovoltaics **9**(2), 123–135 (2001).
[7]F. Wang and N. A. Melosh, Nano Lett. **11**(12), 5426–5430 (2011).
[8]M. W. Knight, Y. Wang, A. S. Urban, A. Sobhani, B. Y. Zheng, P. Nordlander, and N. J. Halas, Nano Lett. **13**(4), 1687–1692 (2013).
[9]F. B. Atar, E. Battal, L. E. Aygun, B. Daglar, M. Bayindir, and A. K. Okyay, Opt. Express **21**(6), 7196–7201 (2013).
[10]T. P. White and K. R. Catchpole, Appl. Phys. Lett. **101**(7), 073905 (2012).
[11]Y. H. Wang, H. Steinberg, P. Jarillo-Herrero, and N. Gedik, Science **342**(6157), 453–457 (2013).
[12]J. Cao, Y. Gao, R. J. D. Miller, H. E. Elsayed-Ali, and D. A. Mantell, Phys. Rev. B **56**(3), 1099 (1997).
[13]M. Bauer, C. Lei, K. Read, R. Tobey, J. Gland, M. M. Murnane, and H. C. Kapteyn, Phys. Rev. Lett. **87**(2), 025501 (2001).
[14]O. O. Ekiz, K. Mizrak, and A. Dana, ACS Nano **4**(4), 1851–1860 (2010).
[15]H. Sezen, A. A. Rockett, and S. Suzer, Anal. Chem. **84**(6), 2990–2994 (2012).
[16]H. Sezen and S. Suzer, J. Vac. Sci. Technol., A **28**(4), 639–642 (2010).
[17]S. Suzer and A. Dana, J. Phys. Chem. B **110**(39), 19112–19115 (2006).
[18]S. Suzer, H. Sezen, and A. Dana, Anal. Chem. **80**(10), 3931–3936 (2008).
[19]S. Ayas, H. Guner, B. Türker, O. O. Ekiz, F. Dirisaglik, A. K. Okyay, and A. Dana, ACS Nano **6**(8), 6852–6861 (2012).
[20]M. L. Huang, Y. C. Chang, Y. H. Chang, T. D. Lin, J. Kwo, and M. Hong, Appl. Phys. Lett. **94**(5), 052106 (2009).
[21]S. Ayas, A. Cupallari, O. O. Ekiz, Y. Kaya, and A. Dana, ACS Photonics **1**(1), 17–26 (2013).
[22]S. Ayas, G. Cinar, A. D. Ozkan, Z. Soran, O. O. Ekiz, D. Kocaay, and A. Dana, Sci. Rep. **3**, 2624 (2013).
[23]H. Chalabi, D. Schoen, and M. L. Brongersma, Nano Lett. **14**(3), 1374–1380 (2014).
[24]G. Ertas, U. K. Demirok, A. Atalar, and S. Suzer, Appl. Phys. Lett. **86**(18), 183110 (2005).
[25]H. Cohen, Appl. Phys. Lett. **85**(7), 1271–1273 (2004).
[26]M. T. Sheldon, J. van de Groep, A. M. Brown, A. Polman, and H. A. Atwater, Science **346**, 828–831 (2014).